

Optical Spectroscopy of Single-Walled Carbon Nanotubes

R. Bruce Weisman

Department of Chemistry, Center for Nanoscale Science and Technology,
and Center for Biological and Environmental Nanotechnology
Rice University, 6100 Main Street, Houston, Texas 77005 USA

1. INTRODUCTION

It has long been known that careful study of the light wavelengths absorbed or emitted from atoms and molecules offers deep insights into their electronic structures. In fact, such optical spectroscopy formed the experimental foundation for the development of quantum mechanics, and it continues to provide precise experimental data essential for understanding the electronic properties of a wide variety of materials. In addition to its central role in basic atomic, molecular, and condensed matter physics, optical spectroscopy has been widely applied in a variety of powerful analytical techniques. These applied spectroscopic methods can sensitively and selectively detect and identify a wide range of chemical substances in varied environments. They currently serve as essential tools in the chemical and pharmaceutical industries, in forensics, in environmental research and safety monitoring, and in medical laboratories. In view of these precedents, researchers in both basic and applied science should take special interest in the optical spectroscopy of novel artificial nanomaterials.

Perhaps the most intensely studied new family of nanomaterials is single-walled carbon nanotubes (SWNT) [1,2]. These are tubular structures of carbon atoms having typical diameters near 1 nm and lengths larger by factors of 100 to 1,000,000. Their extremely high aspect ratios give SWNT some unique and remarkable physical properties. The high aspect ratios also

suggest the need for multidisciplinary approaches in SWNT research: when viewed in cross-section, these nanotubes resemble organic molecules that can be described using concepts and methods of molecular physics; but as viewed along the tube axis, they are extended periodic structures suitable for treatment within condensed matter physics. Although SWNTs are not produced directly from graphite, they can be envisioned as sections of single graphene sheets that have been rolled up to form seamless cylinders capped at the ends with hemi-fullerenes. This rolling up process can generate a large number of discrete transverse structures which differ in tube diameter and chiral (or roll-up) angle. As illustrated in Fig. 1, each of these distinct structures can be described and labeled by the relative position of hexagonal cells in the graphene sheet that become superimposed after roll-up. If one cell is arbitrarily chosen as the origin, then any other can be uniquely identified by two integers, denoted n and m , describing its displacement in primitive lattice vectors from the origin cell. The length of the “roll-up” vector connecting two cells in the graphene sheet equals the circumference of the resulting nanotube, and the angle between that vector and the “zigzag” axis noted in Fig. 1 defines the nanotube’s chiral angle. The long axis of the tube lies perpendicular to the roll-up vector. Chiral angles between 0 and 30° encompass all unique SWNT structures, if enantiomers are neglected.

Each carbon atom in such a single-walled nanotube structure is covalently linked to three neighbors by σ -bonds. The remaining p-electron of each carbon atom joins with those at other sites to form an extended π -electron system whose properties govern SWNT low-energy electronic properties and optical spectroscopy. The available electronic states in this π -system reflect the unusual band structure of graphene combined with the constraint of an angular periodic boundary condition for full rotation about the tube axis. Because this wavefunction boundary condition varies with the (n,m) values describing a nanotube’s construction, each

physical SWNT structure has its own characteristic electronic structure [1,3]. The diversity of electronic properties and their strong dependence on nanotube structure constitute one of the most remarkable and potentially useful features of SWNTs, which must be viewed as a family of related materials rather than a single substance such as C_{60} . It is found that SWNTs for which $n = m$ have a finite density of states at the Fermi energy and display metallic electronic behavior. These structures are called “armchair” nanotubes because of their pattern of bonds around the circumference. Other structures for which the quantity $n - m$ is evenly divisible by 3 are semi-metallic, with band gaps smaller than $k_B T$ at room temperature. The remaining SWNT structures, in which $n - m$ does not divide evenly by 3, are semiconductors. The band gaps of these semiconducting SWNTs vary approximately inversely with nanotube diameter. Nanotubes with the same (n,m) identity but different lengths should have matching optical and electronic properties because SWNT electronic structure is governed by transverse structure. The quasi-one-dimensionality of nanotubes has an important electronic consequence for all (n,m) species: it introduces sharp spikes, called van Hove singularities, into the densities of states.

2. OPTICAL SPECTRA

Fig. 2 shows a band theory model density of states function for a semiconducting SWNT [4]. Each van Hove singularity belongs to a different sub-band, labeled with an integer representing the magnitude of those states’ angular momentum projection along the nanotube axis. Within this model, optical absorption and emission are dominated by dipole-allowed transitions in which light polarized with its electric vector parallel to the tube axis promotes an electron from a valence sub-band to the corresponding conduction sub-band, conserving the angular momentum projection. In a one-electron model, these transitions are predicted to be most intense when the photon energy matches the energy difference between corresponding van

Have singularities. The absorption and emission spectra of a single (n,m) species of SWNT are therefore expected to consist mainly of a series of sharp features at energies E_{ii} , where i takes the values 1, 2, 3, ... according to sub-band. These are illustrated in Fig. 2. For semiconducting SWNTs with diameters near 1 nm, the first three of these transitions will appear in the near-infrared, visible, and near-ultraviolet regions. Metallic or semi-metallic SWNTs of similar diameter will have their lowest energy optical transitions at visible wavelengths falling between the semiconducting nanotubes' E_{22} and E_{33} features. In addition, semi-metallic nanotubes also have much lower energy absorptions in the far-infrared at wavelengths near 100 μm [5,6]. These correspond to transitions across the small, diameter-dependent band gaps (in the range of 10 meV) that are induced by s-p hybridization associated with the nanotubes' cylindrical curvature [7]. Apart from the nondispersive interband optical transitions in the infrared and visible that are characteristic of nanotube diameter and chiral angle, SWNT samples also display dispersive, intense near-ultraviolet absorptions at 4.5 and 5.2 eV that have been assigned to collective plasmon excitations of their π -electrons [8,9].

The near-infrared and visible transitions of SWNTs would be expected to be quite useful in distinguishing different structural species from one another. However, it was found that spectra of samples containing many species typically showed broad, undifferentiated optical absorption features arising from strongly overlapped transitions of those species, rather than sharp, resolved absorptions. In addition, no emission was observed that could be assigned to van Hove interband transitions. A breakthrough in nanotube spectroscopy occurred with the 2002 report of structured absorption from samples of SWNTs that had been prepared with special processing to counteract their strong tendency to form bundles of parallel nanotubes held together by van der Waals forces. To obtain these disaggregated samples, raw and unpurified

product from the HiPco process was first mechanically dispersed into an aqueous solution of a surfactant such as SDS (sodium dodecylsulfate). Then intense ultrasonic agitation was applied to free many individual nanotubes from bundles. Once freed, the nanotubes became surrounded by a micelle-like layer of surfactant molecules that prevented their re-aggregation into bundles. Finally, the sample was subjected to ultracentrifugation, which allowed significant physical separation of suspended individual nanotubes from the slightly denser suspended bundles. Decanted portions of such processed samples showed notably complex and sharpened near-infrared absorption spectra with structure extending from approximately 900 to 1600 nm, as shown in Fig. 3. D₂O was used in preference to H₂O as the solvent for spectroscopic studies because of its superior near-infrared transparency. The isotopic frequency shift of the O-H stretching overtone increases the long wavelength cut-off of D₂O to ca. 1900 nm from 1350 nm in H₂O.

Remarkably, these aqueous samples enriched in individual surfactant-suspended SWNTs also displayed near-infrared photoluminescence. As illustrated in Fig. 4, their highly structured emission spectra show a series of peaks nearly coincident with those in the absorption spectrum. The emission red-shifts are only approximately 4 meV (30 cm⁻¹). This similarity of absorption and emission spectra differs strikingly from the “mirror-image” relation that is common in molecular photophysics [10]. The data show that the sample contains many emitting species, with each displaying one dominant transition in this spectral range and a very small Stokes shift between its absorption and emission peaks. In accord with the predictions of Kasha’s Rule that molecular electronic luminescence originates entirely from the lowest-lying electronic state within a spin multiplicity manifold [11], SWNT emission is observed exclusively for E₁₁ transitions and not for E₂₂ or higher transitions. Clearly, the many distinct spectral features in

the E_{11} region correspond to different (n,m) species of semiconducting single-walled nanotubes in the structurally heterogeneous sample. Precise values of photoluminescence quantum yields are difficult to measure, in part because of overlapping transitions in mixed samples. However, initial estimates suggest quantum yields that are near 10^{-3} and vary somewhat as the nanotube's environment is altered by the presence of different surfactants. It will be of significant interest to quantify the dependence of this yield on nanotube diameter, chiral angle, and extrinsic factors.

Lifetime studies on SWNT optically excited states have been reported by several laboratories [12-16]. Despite some inconsistencies among the measured values, the excited state lifetime of ca. 10^{-10} s can be combined with the emissive quantum yield near 10^{-3} to deduce that the emitting state has a radiative rate constant consistent with a spin-conserving optical transition. Using the terminology of molecular photophysics, nanotube photoluminescence is therefore classified as fluorescence rather than phosphorescence. In the remainder of this chapter, SWNT photoluminescence will be referred to as fluorescence.

3. SPECTROSCOPIC ASSIGNMENT

Once the structured near-infrared emission had been discovered and identified as fluorescent band gap transitions from a variety of semiconducting SWNT species, the crucial next task was spectroscopic assignment: identifying the specific nanotube structure responsible for each peak. The key experimental method used in this task was spectrofluorimetry. Here the emission intensity of a sample was measured as a function of two variables: excitation wavelength and emission wavelength. The excitation source's wavelength was scanned over the range of E_{22} transitions, and when the photon energy matched the second van Hove transition energy of one of the SWNT species in the sample, the resulting optical absorption generated a hole in its second valence sub-band and an electron in its second conduction sub-band. The

electrons and holes relaxed through phonon emission to the first sub-bands. Then a small fraction of the excited nanotubes emitted E_{11} near-infrared fluorescence through radiative electron-hole recombination across the semiconducting band gap. The wavelength of this emission was characteristic of the nanotube species that had undergone resonant E_{22} excitation. Fig. 5 displays the results from this experiment in the form of a surface plot, where height corresponds to emission intensity and the two other axes represent excitation and emission wavelengths. A rich structure of “mountain peaks” is clearly evident for excitation in the E_{22} range between ca. 500 and 800 nm. Each of these peaks arises from a distinct (n,m) species of semiconducting nanotube. The unique E_{11} and E_{22} transition energies of each species may be found immediately from the wavelength coordinates of its peak.

The data shown in Fig. 5 immediately provided a valuable correlation E_{11} and E_{22} values for many different nanotube species. However, assignment to the correct (n,m) values required extensive further analysis. Fig. 6 shows a plot of experimental E_{22}/E_{11} ratios as a function of excitation wavelength (inversely proportional to E_{22}). The data points appear to form a systematic splay pattern, as illustrated by the solid lines. This remarkable, regular pattern of spectral data must reflect the systematic pattern of nanotube structures present in the sample. The connection between structural and spectral patterns was found by comparing the experimental findings with a similar plot of results from an extended tight-binding model computation. Although there was no quantitative match of ratios or excitation wavelengths between this model and experiment, the model revealed a qualitatively similar splay pattern. In this pattern, points on a given line share the same value of $n-m$, and both n and m increase by one from left to right between adjacent points along any splay line. We take the value of $n-m$ to define a “family” of nanotube structures. Note that because only semiconducting SWNTs emit

fluorescence, no points or lines are present for $n-m$ family values of 0, 3, 6, 9, ..., which correspond to metallic or semi-metallic species. The quantitative changes in n and m along a dotted line path connecting adjacent splay lines were also deduced by comparison with the model calculations. In this way, the connectivity pattern determining relative n and m values for the entire network of experimental spectroscopic points was deciphered. However, additional work was needed to assign absolute values of n and m .

The range of “anchoring” choices to define absolute (n,m) values was limited to a handful of plausible candidates by considerations such as the distribution of nanotube diameters that had previously been found from TEM analysis of the measured SWNT sample. Raman spectroscopy was then used to select the correct choice from among these candidates. Prior experimental and theoretical studies had found that the low-frequency radial breathing vibrational mode (RBM) is strongly resonance enhanced in SWNT Raman spectra, and that its frequency is inversely related to nanotube diameter [17-20]. Raman spectroscopy was performed using a variety of laser wavelengths that provided resonance with ten different E_{22} transitions of semiconducting nanotubes in the surfactant-suspended SWNT sample. This gave a set of experimental RBM frequencies correlated with E_{22} transition wavelengths. Each candidate anchoring choice assigned different (n,m) values, and therefore different diameters, to the ten species in this set on the basis of their optical transitions. For each candidate anchoring choice, the experimental RBM frequencies were plotted vs. those purported inverse diameters. These plots were then compared for linearity. One choice was clearly superior in satisfying the expected linear relation between RBM frequency and inverse nanotube diameter, and that choice was therefore identified as the correct spectral assignment. Once the assignment was deduced, the (n,m) identities of all 33 observed peaks in Fig. 5 were immediately revealed. This provided precise experimental E_{11}

and E_{22} transition energies for a large set of semiconducting nanotube species spanning a substantial range of diameters and chiral angles. Fig. 7 shows the identified and labeled E_{11} and E_{22} wavelengths for SWNTs in aqueous SDS suspension.

4. FURTHER OBSERVATIONS

The discovery and structural assignment of nanotube fluorescence has triggered a large wave of spectroscopically-based studies of SWNT physical and chemical properties. Not surprisingly, these further investigations have revealed greater complexity than is implied by the simple model presented above. For example, the electron and hole formed by optical excitation are not independent, as implied by the single-particle band structure sketch of Fig. 2. Instead, they remain spatially associated as an exciton with a binding energy that is much larger than would be expected in a comparable three-dimensional material. This excitonic character of nanotube optically excited states, which has a parallel in the electronic excitations of “zero-dimensional” molecular systems, has been predicted and modeled in several theoretical studies [21-29]. Early experimental evidence of nanotube excitons was seen in the shape of fluorescence excitation features, which are nearly symmetric Lorentzians rather than the asymmetric profiles expected from the joint density of one-electron states in a one-dimensional system [4,30]. A number of subsequent experimental studies have provided clear corroboration and much more detailed information about SWNT excitons [12,15,31-36]. Theoretical predictions of exciton binding energies that approach 40% of the tight-binding energy gap [23] seem to be supported by experimentally deduced binding energy values near 0.4 eV for smaller diameter species [34,35]. It therefore seems surprising that one-electron band theory models, which neglect excitonic effects, are fairly successful in describing nanotube optical transition energies. This success apparently reflects the approximate cancellation of two large but

opposing many-body effects: electronic self-energy and exciton binding energy [26,27]. In addition, the van Hove-dominated interband optical transitions that are expected from a band theory picture and illustrated in Fig. 2 are transformed by inclusion of excitonic effects into a single dominant transition for each matching pair of sub-bands in a given (n,m) species. Thus, the use of E_{ij} labels to classify optical transitions and the simple correspondences between species and transition wavelengths remain valid in excitonic treatments of nanotube spectroscopy.

Another example of spectral complexity is the presence of low-intensity absorption or emission features that are distinct from a nanotube species's dominant van Hove transitions. Some of these secondary features can be assigned to transitions with simultaneous changes in a nanotube's electronic and vibrational states, equivalent to vibronic transitions in molecules or phonon side-bands in solid state spectroscopy [15,37]. Others may reflect transitions to higher-energy excitonic states [15,35]. Energy transfer between different species of semiconducting nanotubes can give emission at the acceptor's wavelength following excitation of a transition in the energy donor. Finally, some weak optical features may also be assignable to E_{ij} cross-transitions between different sub-bands [38]. In contrast to the dominant E_{ij} features, selection rules for such cross-transitions require the light to be polarized perpendicular to the nanotube axis. The systematic observation and assignment of cross-transitions will provide important new insights into nanotube band structure and many-body effects.

Fluorescence appears to be the optical property of nanotubes that is most sensitive to sample condition. The most obvious example of this is the virtual absence of near-IR emission from nanotubes that have aggregated into bundles held together by van der Waals forces. It seems likely that this effect arises from efficient energy transfer within the bundle. Statistically,

approximately one-third of the nanotubes in a raw sample are expected to be metallic. There is therefore a high probability that randomly formed bundles containing at least several nanotubes will include one or more metallic tubes. When a bundled semiconducting SWNT absorbs light, electronic coupling with its neighbors causes excitation transfer to species with smaller band gaps and eventually to a metallic nanotube, in which the excitation must relax nonradiatively. This efficient fluorescence quenching process allows one to use emissive yield as a sensitive monitor of SWNT aggregation.

Variations of fluorescence quantum yield with temperature reflect the combined temperature dependencies of competing radiative and nonradiative decay channels. In nanotubes, these channels include nonradiative relaxation from the optically excited state (generally E_{22} or higher) to the E_{11} excited state, and subsequent decay of the E_{11} excitation through either radiative emission or nonradiative relaxation. Recent considerations of “dark” nanotube exciton states, which have optical transitions to the ground state that are forbidden by symmetry selection rules or by triplet spin character, suggest that both radiative and nonradiative processes in nanotubes may depend strongly on phonon population, and therefore on temperature [39,40]. Experimentally, it has been reported that certain SWNT species show more than an order of magnitude intensification of their fluorescence emission as samples are cooled from ambient to cryogenic temperatures [41,42]. Further studies along these lines will surely prove important for basic and applied nanotube research.

Fluorescence efficiency can also be sensitive to chemical environment. The addition of acid to aqueous suspensions of pristine SWNT in ionic surfactants causes fluorescence quenching that can be reversed by the addition of base to restore pH to a neutral or alkaline value [43-45]. Such quenching differs from the complete and essentially irreversible loss of near-

infrared fluorescence caused by many oxidative acid treatments that are commonly applied to raw SWNT material to remove residual metallic catalysts. (This is why nanotube fluorescence was discovered only through the use of “unpurified” samples.) In addition, many chemical reactions that derivatize nanotube sidewalls inhibit fluorescence. It seems likely that the perturbation of a nanotube’s π -electron system by the chemical conversion of scattered carbon atoms from sp^2 to sp^3 hybridization produces sites for efficient nonradiative recombination of excitons. Although such chemical derivatization also leads to the characteristic D-band in Raman spectra and the loss of van Hove structure in electronic absorption spectra, fluorescence is lost significantly before the onset of these other spectroscopic symptoms. This high sensitivity of fluorescence quantum yield to sidewall defects may reflect the mobility of excitons along the tube axis. Through such motion the electronic excitation can visit relatively large segments of a nanotube during its lifetime and undergo efficient quenching by sparse defect sites.

Another important effect is the sensitivity to external environment of SWNT optical transition energies. With every carbon atom occupying a surface site, SWNTs more closely resemble molecules than solids in terms of exposure to surroundings. It is therefore not surprising that nanotubes should mimic the well-known spectral variations observed for a molecular solute dissolved in different solvents. One would expect E_{11} transitions to be more environmentally sensitive than the E_{22} , E_{33} , ... transitions, which involve deeper valence states that are analogous to core orbitals and interact more weakly with the surroundings. In fact, such a pattern seems to be present in the limited systematic observations reported to date. Data are available for E_{11} and E_{22} transitions of SWNT that are dissolved in polymeric films, or suspended in air between pillars over a silicon surface [46,47], or in water surrounded by various surfactants [48]. It appears that E_{11} transitions red-shift by ca. 28 meV and E_{22} transitions by ca.

16 meV in aqueous SDS suspension as compared to an air environment [46]. These represent relative transition energy changes of approximately -3% and -1% for E_{11} and E_{22} . When SDS or SDBS is replaced by other synthetic surfactants, E_{11} red-shifts of up to 3% are observed.

Finally, when biopolymers such as proteins or DNA are used as aqueous suspending agents, SWNT E_{11} transitions shift still further to lower energies [49,50]. However, because these overall environmental spectral shifts are relatively small and seem to be fairly systematic, it is feasible to adapt the (n,m) assignments deduced from aqueous SDS suspensions to assign spectral features in other media. Furthermore, the limited magnitudes of environmental shifts provide confidence that spectral patterns revealed in studies of aqueous suspensions reflect the intrinsic electronic properties of SWNTs.

Nanotube environment also affects the observed emission line widths. The smallest full-widths at half-maximum normally found in bulk aqueous suspensions are approximately 22 meV with ionic surfactants SDBS and sodium cholate. Non-ionic polymeric surfactants such as Pluronic broaden fluorescence features by ca. 35%, and biopolymers can give comparable or even greater broadening. The SWNT emission profiles reflect both homogeneous (Lorentzian) and inhomogeneous (Gaussian) broadening components. Nearly Lorentzian emission profiles have been observed from individual nanotubes at ambient temperature [47,51]. Microscopic studies on dilute SWNT in polymeric films have recently revealed small (ca. 3 meV) differences in the emission peak position between opposite ends of a slightly bent single nanotube [52]. This illustrates that inhomogeneous spectral broadening can occur within a single nanotube, as different segments along the tube's axis act as independent fluorophores. Polarization-dependent measurements in the same report confirmed that optically generated excitons were not able to travel ca. 3 μm between the ends of a bent SWNT during their lifetime [52]. Studies at

cryogenic temperatures have found complex spectral behavior, with SWNT emission line widths as narrow as 1 meV and multiple peak positions from a single nanotube type [42,53]. This behavior may reflect the trapping of excitons along the tube axis because of reduced mobility at very low temperatures. Temperature-dependent studies of bulk SWNT suspensions have shown that cooling causes the pattern of transition frequencies shown in Fig. 6 to become even more splayed, with systematic, (n,m) -dependent changes in E_{11} and E_{22} [41]. These complex and reversible spectral shifts, in which some transition frequencies increase while others decrease, have been attributed to non-uniform nanotube strain induced by thermal contraction or expansion of the host medium. By contrast, the application of isotropic hydrostatic pressure at fixed temperature induces spectral displacements that vary with (n,m) but shift consistently to lower frequency [54].

5. SPECTROSCOPIC APPLICATIONS

5.1 SWNT Electronic Structure Elucidation

Although the visible and near-infrared optical transitions of nanotubes in aqueous surfactant suspension are broad by the standards of gas phase molecular spectroscopy, their center frequencies can often be measured to a relative precision of ca. 0.2% or 0.1%, respectively. Fig. 8 shows measured transition wavelengths as a function of deduced nanotube diameter. The experimental precision is sufficient to reveal novel patterns in SWNT electronic structure and severely challenge many approximate theoretical models. For example, the experimental variations in transition energies with chiral angle significantly exceed the trigonal warping effects predicted from simple tight binding modeling. Fig. 8 also shows the segregation of semiconducting SWNT families into two groups. In one of these groups the value of $\text{mod}(n-m,3)$ equals 1, while in the other group it equals 2. As expected, the E_{22}/E_{11} ratios found from

spectral data vary with diameter, chiral angle, and mod $(n-m,3)$ group, but Fig. 9 shows that the measured ratios extrapolate to a value near 1.8 in the limit of armchair chirality, rather than to the value of 2 predicted by band theory models. This discrepancy, termed the “ratio problem” [22], has spurred incisive efforts to compute and understand the role of many-body effects in SWNT spectroscopy [22,26-28,55,56]. The spectroscopic findings are thus playing a valuable role in stimulating and guiding the refinement of nanotube electronic structure theories.

5.2 SWNT Sample Characterization

The difficulty of sample characterization currently poses a serious obstacle to progress in nanotube basic research, applied research, and commercialization. In addition to their important use in elucidating basic nanotube physics, structure-assigned optical spectra have major value for such nanotube sample analysis. One of these applications involves the widespread use of resonance Raman spectroscopy as a characterization tool. In this method the Raman excitation laser must have a photon energy quite close to an E_{ii} optical resonance in order to generate conveniently intense scattering signals, so it is necessary to select laser wavelengths appropriate for the SWNT species of interest. Such matching of nanotube diameters to E_{ii} values has generally been guided by “Kataura plots” representing parameterized tight-binding model calculations. The spectroscopically determined transition energies have now been accurately fit to empirical functions of diameter and chiral angle to permit reliable extrapolation to a wide range of semiconducting species [57]. When these empirically based values for semiconducting E_{11} and E_{22} transitions are compared with Kataura plots based on simple tight-binding calculations, significant errors of ca. 15% are apparent, as can be seen from Fig. 10. The model plots seriously underestimate the E_{11} transition energies and the variation of those energies with chiral angle. The empirically-based plot of E_{11} and E_{22} transition energies vs. diameter therefore

offers much more reliable guidance for many Raman nanotube investigations. It also serves as a reference for calibrating enhanced theoretical models that will be useful for predicting optical transitions of metallic nanotubes and higher van Hove transitions of semiconducting species.

The most powerful analytical application of structure-assigned optical spectra uses fluorimetry to deduce the detailed composition of SWNT samples. Recall that nearly all SWNT samples contain nanotubes with a variety of diameters and chiral angles. Following optical excitation in an E_{22} or higher transition, each semiconducting species in a sample will emit near-infrared light at a wavelength characteristic of its (n,m) identity. By measuring this emission intensity as a function of excitation and emission wavelengths and using the optical assignment findings described above to identify the (n,m) species corresponding to each peak, one can compile an inventory of semiconducting nanotube species present in the sample.

In many applications, it is useful to have quantitative analyses in addition to a qualitative inventory. True quantitation is challenging because nanotube species may differ as to absorptivities in the excitation transition and quantum yields for E_{11} emission. However, if one assumes that these variations are minor over the range of structures present in a given sample, then the relative concentrations of (n,m) species may be directly deduced from their fluorescence intensities. This assumption is supported by the expectation that systematic variations in optical factors with structure will reverse sign between E_{11} and E_{22} transitions, giving partial cancellation of fluorimetric sensitivity variations for E_{22} excitation and E_{11} detection. We note that estimating a bulk sample's (n,m) composition from resonance Raman spectroscopy is much more challenging because of the need to use a wide variety of exciting laser wavelengths, the likelihood that Raman cross-sections depend strongly on diameter and chirality, and the double involvement of a single E_{ii} transition. An important near-term goal for the field of nanotube

fluorimetry is to calibrate optical signal strengths against independently measured species concentrations so as to enable convenient quantitative (n,m) -level analyses.

Barriers to using fluorimetry as a routine tool for bulk sample characterization have included cumbersome instrumentation, relatively slow data collection, and manual data interpretation. Fortunately, these drawbacks have recently been overcome. Although a full two-dimensional scan of emission intensity as a function of excitation and emission wavelengths offers the most complete fluorimetric characterization, it is in fact practical to obtain nearly equivalent information from just two or three emission spectra excited by discrete, well-chosen wavelengths. This approach exploits the relatively large Lorentzian widths of nanotube E_{22} transitions to achieve off-resonance excitation of numerous species using a fixed monochromatic light source. Instrumentation designed for efficient fluorimetric analysis may contain diode lasers for E_{22} excitation and a near-IR spectrograph with multichannel detector for capturing emission spectra without wavelength scanning. The lasers provide excitation intensities several orders of magnitude higher than monochromated arc lamp sources, while occupying less much laboratory space. An instrument of this type can acquire very high quality emission spectra from typical aqueous SWNT dispersions quite quickly. Fig. 11 shows such a fluorescence spectrum measured with an acquisition time of only 500 ms.

Because the monochromatic diode lasers excite a variety of (n,m) species, sample emission spectra show complex superpositions of peaks representing the E_{11} fluorescence of many semiconducting nanotube structures. To interpret such spectra, one applies prior spectroscopic knowledge of the E_{11} peak emission frequencies for those (n,m) species that may be present in the sample. Using additional information about the typical Voigt emission line profiles, a measured spectrum may be quickly computer-simulated as a sum of individual species

components to obtain the sample's (n,m) inventory. Relative amplitudes deduced in this fitting will not match those from peaks in full two-dimensional spectrofluorimetry until they have been adjusted by factors reflecting the mismatch between the laser wavelength used for excitation and the peak E_{22} wavelengths of the (n,m) species. After applying such adjustment factors, however, one obtains a sample analysis comparable to that from two-dimensional data, except with much faster data collection. Moreover, both the data acquisition and spectral data analysis can be automated to allow routine, rapid sample characterization with minimal operator input or expertise. Because this method relies on SWNT fluorescence, it is not suitable for observing metallic or semi-metallic SWNT species, bundled nanotubes, or nanotubes that have been substantially chemically damaged or derivatized. It is most effective for deducing the (n,m) content of samples containing smaller diameter SWNT (below ca. 1.2 nm), for which the average separation between E_{11} frequencies is large enough to avoid severe spectral congestion in emission. However, fluorescence analysis can also be used with larger diameter samples to deduce diameter distributions without resolving populations at the level of individual (n,m) species. It appears that the development of commercialized automated systems for fluorimetric SWNT analysis will provide a valuable new characterization tool for a wide range of laboratories engaged in nanotube basic research, applications development, or production quality control.

5.3 SWNT Detection and Imaging

An emerging application of SWNT fluorescence exploits near-infrared fluorescence to detect the presence of nanotubes and visualize their locations. Although the emissive quantum yield of nanotubes (as estimated from aqueous dispersions) seems to be only near 10^{-3} , their emission lies in a spectral region that is nearly free of luminescent background from natural materials. This absence of emissive background interference plus the characteristic spectral

signature of SWNT fluorescence make it possible to selectively detect very small relative concentrations of nanotubes embedded in complex sample environments. Fluorescence detection is therefore an appealing approach to finding and quantifying trace amounts of pristine SWNTs in environmental or biological specimens. As the remarkable properties of SWNTs lead in the future to increased and possibly large-scale use in industrial products, concerns will arise about nanotube safe disposal and possible environmental impact. Effective methods of analysis will be needed to address such concerns. SWNT analytical methods will also be essential for studying the fate of nanotubes introduced into organisms through unintended exposure or through administration of nanotube-based medical agents.

Analytical options are quite limited for such specimens. Because of the high carbon content in the surroundings, SWNTs obviously cannot be determined by elemental analysis. High resolution microscopies such as TEM, STM, and AFM are extremely useful for observing nanotubes in clean samples on specialized substrates, but they face the problem of finding a “carbon needle in a haystack” for specimens dense with complex organic components or biopolymers. Radiotracer methods would be effective but probably require the preparation of SWNT samples containing ^{14}C , a difficult task. Like fluorescence, resonance Raman spectroscopy offers sensitivity down to the single-nanotube level [58]. However, the resonance-enhanced Raman signals from tiny fractional concentrations of SWNT can be obscured by overlapping background fluorescence, intense elastic scattering, or non-resonant Raman scattering from other molecular species that comprise the bulk of the sample. By comparison, near-IR SWNT fluorescence is conveniently excited by E_{22} transitions, which typically lie ca. 5000 cm^{-1} above the E_{11} emission. Because of this large shift, which exceeds the fundamental Raman frequencies of any organic compound, there is no Raman scattering interference at the

wavelengths used to detect SWNT fluorescence. Furthermore, endogenous or background luminescence from biological materials is extremely weak at the relevant detection wavelengths beyond ca. 1100 nm. These factors currently enable detection of SWNT emission with high signal-to-background ratios from cells and tissues that contain nanotubes at parts-per-million concentrations. Substantially improved sensitivity and selectivity will be attained in the future by using specially grown or sorted SWNT samples composed mainly of individual semiconducting (n,m) species [59]. With such samples, optical efficiency can be greatly enhanced through the use of resonant excitation wavelengths and narrow-band spectral filtering of emission.

A particularly exciting development is the use of near-infrared fluorescence microscopy to visualize the locations of pristine (underivatized) nanotubes in media including solid films, liquid suspensions, and biological cells and tissues[50,52]. Because much of the SWNT emission lies at wavelengths beyond the range of silicon-based cameras, it is necessary to use relatively exotic imagers built from arrays of InGaAs photodiodes. These detectors have the disadvantages of high cost, low resolution, imperfections, and high dark current, but they provide high quantum efficiencies for detection within the 900 to 1600 nm range typical of many SWNT samples. A conventional optical microscope can be relatively simply adapted for SWNT microscopy by adding a diode laser suitable for sample excitation, appropriate filters and dichroic optics, and the near-IR imager. Fig. 12 is a near-IR fluorescence micrograph recorded from emission between 1125 to 1600 nm using such a modified microscope. The image shows nanotube fluorescence from a macrophage-like cell that had been incubated in a growth medium containing suspended SWNT [50]. Two significant findings are immediately evident. First, the luminescent nanotubes are not uniformly distributed throughout the cell's cytoplasm but are

instead concentrated in a number of small intracellular structures. These are believed to be phagosomes. Second, areas of the cytoplasm outside of these structures appear as dark as the region surrounding the cell, indicating the very low level of endogenous fluorescence background in the observed spectral range and the resulting excellent contrast attained despite the low quantum yield of SWNT emission. By adapting a confocal scanning microscope for near-IR nanotube detection, it should be possible in the future to improve spatial resolution by the ratio of emission to excitation wavelengths, a factor of approximately 2, although at some cost in data acquisition time.

Near-IR fluorescence imaging appears to be rapidly evolving into a practical method for visualizing the distributions of SWNTs inside biological cells, tissues, and even intact organisms. This application is favored by the reported steady fluorescence from nanotubes under conditions that cause rapid photobleaching of organic fluorophores or blinking between on and off states in inorganic quantum dots [51], and also by the weaker absorption and scattering in tissues of near-IR as compared to visible light. It should soon prove possible to monitor the location, orientation, and motions of single SWNTs in cells through *in vitro* near-IR fluorescence microscopy. If covalent or noncovalent derivatization methods can be developed that allow nanotubes to remain fluorescent after linkage to biological targeting agents such as antibodies or peptides, then SWNTs may form the basis for a new class of near-IR bio-markers useful in laboratory research. Targeted nanotubes may also have potential as near-IR fluorescent contrast agents that could be noninvasively detected or imaged from inside human patients to enable novel modes of medical diagnosis.

6. SUMMARY

Single-walled carbon nanotubes form a family of artificial nanomaterials with a rich, unusual, and useful array of optical spectroscopic properties. Each structural species of semiconducting nanotube displays not only a set of intense and distinct absorption transitions ranging from near-infrared to ultraviolet wavelengths, but also well-defined fluorescent band-gap photoluminescence in the near-infrared. The discovery of this fluorescence emission allowed the complex superposition spectra shown by structurally mixed nanotube samples to be dissected by spectrofluorimetric experiments and then deciphered by careful data analysis. A large set of absorption and emission features were thereby successfully assigned to specific structural species of nanotubes. The results provide a valuable body of precise experimental data that have led to greatly improved understanding of nanotube electronic structure and the role of many-body effects in their optically excited states. The secure assignment of spectral features to nanotube structures has also formed the basis for efficient optically-based methods for deducing the detailed composition of bulk nanotube mixtures. These new analytical tools should support and accelerate progress in basic research, applied research, and commercial use of carbon nanotubes. Finally, the unusual near-infrared fluorescence wavelengths of semiconducting nanotubes enhance the value of emission methods for detecting and visualizing nanotubes in complex environmental and biological specimens. Active research projects underway in many laboratories are advancing nanotube chemical modification, near-infrared imaging instrumentation, and knowledge of nanotube-biological interactions. Supported by progress in these areas, the unique optical properties of single-walled carbon nanotubes may eventually let them play important roles in medical research and clinical applications.

ACKNOWLEDGEMENTS

The author gratefully acknowledges the vital creative contributions of his co-workers and collaborators, and research support from National Science Foundation (grant CHE-0314270), Rice's NSF-supported Center for Biological and Environmental Nanotechnology (under grant EEC-0118007) and the Welch Foundation (grant C-0807).

REFERENCES

- [1] R.Saito, G.Dresselhaus, M.S.Dresselhaus, *Physical Properties of Carbon Nanotubes*, Imperial College Press, London, 1998.
- [2] M. S. Dresselhaus, G. Dresselhaus, and Ph. Avouris (eds.), *Carbon Nanotubes: Synthesis, Structure, Properties, and Applications*, Springer-Verlag, New York, 2001.
- [3] S.Reich, J.Janina, C.Thomsen, *Carbon Nanotubes: Basic Concepts and Physical Properties*, Wiley, New York, 2004.
- [4] J. W. Mintmire, C. T. White, Universal density of states for carbon nanotubes, *Phys. Rev. Lett.* 81 (1998) 2506 - 2509.
- [5] A. Ugawa, A. Rinzler, D. B. Tanner, Far-infrared gaps in single-wall carbon nanotubes, *Phys. Rev. B* 60 (1999) R11305 - R11308.
- [6] M. E. Itkis, S. Niyogi, M. E. Meng, M. A. Harmon, H. Hu, R. C. Haddon, Spectroscopic study of the Fermi level electronic structure of single-walled carbon nanotubes, *Nano Lett.* 2 (2002) 155 - 159.
- [7] C. L. Kane, E. J. Mele, Size, shape, and low energy electronic structure of carbon nanotubes, *Phys. Rev. Lett.* 78 (1997) 1932 - 1935.
- [8] Th. Pichler, M. Knupfer, M. S. Golden, J. Fink, A. Rinzler, R. E. Smalley, Localized and delocalized electronic states in single-wall carbon nanotubes, *Phys. Rev. Lett.* 80 (1998) 4729 - 4732.
- [9] Y. Murakami, E. Einarsson, T. Edamura, S. Maruyama, Polarization dependence of the optical absorption of single-walled carbon nanotubes, *Phys. Rev. Lett.* 94 (2005) 087402/1 - 087402/4.
- [10] J.B.Birks, *Photophysics of Aromatic Molecules*, Wiley, London, 1970.
- [11] M. Kasha, Characterization of electronic transitions in complex molecules, *Disc. Faraday Soc.* 9 (1950) 14 - 19.
- [12] Y.-Z. Ma, J. Stenger, J. Zimmerman, S. M. Bachilo, R. E. Smalley, R. B. Weisman, G. R. Fleming, Ultrafast carrier dynamics in single-walled carbon nanotubes probed by femtosecond spectroscopy, *J. Chem. Phys.* 120 (2004) 3368 - 3372.
- [13] G. N. Ostojic, S. Zaric, J. Kono, M. S. Strano, V. C. Moore, R. H. Hauge, R. E. Smalley, Interband Recombination Dynamics in Resonantly Excited Single-Walled Carbon Nanotubes, *Phys. Rev. Lett.* 92 (2004) 117402/1 - 117402/4.
- [14] S. Reich, M. Dworzak, A. Hoffmann, C. Thomsen, M. S. Strano, Excited-state carrier lifetime in single-walled carbon nanotubes, *Phys. Rev. B* 71 (2005) 033402/1 - 033402/4.

- [15] M. Jones, C. Engtrakul, W. K. Metzger, R. J. Ellingson, A. J. Nozik, M. J. Heben, G. Rumbles, Analysis of photoluminescence from solubilized single-walled carbon nanotubes, *Phys. Rev. B* 71 (2005) 115426/1 - 115426/9.
- [16] J.-P. Yang, M. M. Kappes, H. Hippler, A.-N. Unterreiner, Femtosecond transient absorption spectroscopy of single-walled carbon nanotubes in aqueous surfactant suspensions: determination of the lifetime of the lowest excited state, *Physical Chemistry Chemical Physics* 7 (2005) 512 - 517.
- [17] A. M. Rao, E. Richter, S. Bandow, B. Chase, P. C. Eklund, K. A. Williams, S. Fang, K. R. Subbaswamy, M. Menon, A. Thess, R. E. Smalley, G. Dresselhaus, M. S. Dresselhaus, Diameter-selective Raman scattering from vibrational modes in carbon nanotubes, *Science* 275 (1997) 187 - 191.
- [18] M. S. Dresselhaus, G. Dresselhaus, A. Jorio, A. G. Souza Filho, R. Saito, Raman spectroscopy on isolated single wall carbon nanotubes, *Carbon* 40 (2002) 2043 - 2061.
- [19] S. Bandow, S. Asaka, Y. Saito, A. M. Rao, L. Grigorian, E. Richter, P. C. Eklund, Effect of the growth temperature on the diameter distribution and chirality of single-wall carbon nanotubes, *Phys. Rev. Lett.* 80 (1998) 3779 - 3782.
- [20] G. S. Duesberg, W. J. Blau, H. J. Byrne, J. Muster, M. Burghard, L. J. Rothberg, S. Roth, Experimental observation of individual single-wall nanotube species by Raman microscopy, *Chem. Phys. Lett.* 310 (1999) 8 - 14.
- [21] T. Ando, Excitons in carbon nanotubes, *J. Phys. Soc. Jpn.* 66 (1997) 1066 - 1073.
- [22] C. L. Kane, E. J. Mele, Ratio problem in single carbon nanotube fluorescence spectroscopy, *Phys. Rev. Lett.* 90 (2003) 207401/1 - 207401/4.
- [23] T. G. Pedersen, Variational approach to excitons in carbon nanotubes, *Phys. Rev. B* 67 (2003) 073401/1 - 073401/4.
- [24] E. Chang, G. Bussi, A. Ruini, E. Molinari, Excitons in carbon nanotubes: an ab initio symmetry-based approach, *Phys. Rev. Lett.* 92 (2004) 196401/1 - 196401/4.
- [25] H. Zhao, S. Mazumdar, Electron-electron interaction effects on the optical excitations of semiconducting single-walled carbon nanotubes, *Phys. Rev. Lett.* 93 (2004) 157402/1 - 157402/4.
- [26] C. L. Kane, E. J. Mele, Electron interactions and scaling relations for optical excitations in carbon nanotubes, *Phys. Rev. Lett.* 93 (2004) 197402/1 - 197402/4.
- [27] C. D. Spataru, S. Ismail-Beigi, L. X. Benedict, S. G. Louie, Excitonic effects and optical spectra of single-walled carbon nanotubes, *Phys. Rev. Lett.* 92 (2004) 077402/1 - 077402/4.

- [28] V. Perebeinos, J. Tersoff, Ph. Avouris, Scaling of excitons in carbon nanotubes, *Phys. Rev. Lett.* 92 (2004) 257402/1 - 257402/4.
- [29] V. Perebeinos, J. Tersoff, Ph. Avouris, Electron-phonon interaction and transport in semiconducting carbon nanotubes, *Phys. Rev. Lett.* 94 (2005) 086802/1 - 086802/4.
- [30] M. O'Connell, S. M. Bachilo, C. B. Huffman, V. Moore, M. S. Strano, E. Haroz, K. Rialon, P. J. Boul, W. H. Noon, C. Kittrell, J. Ma, R. H. Hauge, R. B. Weisman, R. E. Smalley, Band-gap fluorescence from individual single-walled carbon nanotubes, *Science* 297 (2002) 593 - 596.
- [31] C. Manzoni, A. Gambetta, E. Menna, M. Meneghetti, G. Lanzani, G. Cerullo, Intersubband exciton relaxation dynamics in single-walled carbon nanotubes, *Phys. Rev. Lett.* 94 (2005) 207401/1 - 207401/4.
- [32] S. G. Chou, F. Plentz, J. Jiang, R. Saito, D. Nezich, H. B. Ribeiro, A. Jorio, M. A. Pimenta, G. G. Samsonidze, A. P. Santos, M. Zheng, G. B. Onoa, E. D. Semke, G. Dresselhaus, M. S. Dresselhaus, Phonon-assisted excitonic recombination channels observed in DNA-wrapped carbon nanotubes using photoluminescence spectroscopy, *Phys. Rev. Lett.* 94 (2005) 127402/1 - 127402/4.
- [33] C.-X. Sheng, Z. V. Verdeny, A. B. Dalton, R. H. Baughman, Exciton dynamics in single-walled nanotubes: transient photoinduced dichroism and polarized emission, *Phys. Rev. B* 71 (2005) 125427/1 - 125427/11.
- [34] Y.-Z. Ma, L. Valkunas, S. L. Dexheimer, S. M. Bachilo, G. R. Fleming, Femtosecond spectroscopy of optical excitations in single-walled carbon nanotubes: evidence for exciton-exciton annihilation, *Phys. Rev. Lett.* 94 (2005) 157402/1 - 157402/4.
- [35] F. Wang, G. Dukovic, L. E. Brus, T. F. Heinz, The optical resonances in carbon nanotubes arise from excitons, *Science* 307 (2005) 838 - 841.
- [36] X. Qiu, M. Freitag, V. Perebeinos, Ph. Avouris, Photoconductivity spectra of single-wall carbon nanotubes: implications on the nature of their excited states, *Nano Lett.* 5 (2005) 749 - 752.
- [37] H. Htoon, M. J. O'Connell, S. K. Doorn, V. I. Klimov, Single carbon nanotubes probed by photoluminescence excitation spectroscopy: the role of phonon-assisted transitions., *Phys. Rev. Lett.* 94 (2005) 127403/1 - 127403/4.
- [38] S. Maruyama, to be published (2005).
- [39] C. D. Spataru, S. Ismail-Beigi, R. B. Capaz, S. G. Louie, Theory and ab initio calculation of radiative lifetime of excitons in semiconducting carbon nanotubes, Los Alamos National Laboratory, Preprint Archive, Condensed Matter (2005) 0507067/1 - 0507067/12.

- [40] V. Perebeinos, J. Tersoff, Ph. Avouris, Radiative lifetime of excitons in carbon nanotubes, Los Alamos National Laboratory Preprint Archive, Condensed Matter (2005) 0506775/1 - 0506775/4.
- [41] K. Arnold, S. Lebedkin, O. Kiowski, F. H. Hennrich, M. M. Kappes, Matrix-imposed stress-induced shifts in the photoluminescence of single-walled carbon nanotubes at low temperatures, *Nano Lett.* 4 (2004) 2349 - 2354.
- [42] J. Lefebvre, P. Finnie, Y. Homma, Temperature-dependent photoluminescence from single-walled carbon nanotubes, *Phys. Rev. B* 70 (2004) 045419/1 - 045419/8.
- [43] M. S. Strano, C. B. Huffman, V. C. Moore, M. J. O'Connell, E. H. Haroz, J. Hubbard, M. Miller, K. Rialon, C. Kittrell, S. Ramesh, R. H. Hauge, R. E. Smalley, Reversible, Band-gap-selective protonation of single-walled carbon nanotubes in solution, *J. Phys. Chem. B* 107 (2003) 6979 - 6985.
- [44] G. Dukovic, B. E. White, Z. Y. Zhou, F. Wang, S. Jockusch, M. L. Steigerwald, T. F. Heinz, R. A. Friesner, N. J. Turro, L. E. Brus, Reversible surface oxidation and efficient luminescence quenching in semiconductor single-wall carbon nanotubes, *J. Am. Chem. Soc.* 126 (2004) 15269 - 15276.
- [45] R. B. Weisman, S. M. Bachilo, D. Tsyboulski, Fluorescence spectroscopy of single-walled carbon nanotubes in aqueous suspension, *Applied Physics A* 78 (2004) 1111 - 1116.
- [46] J. Lefebvre, J. M. Fraser, Y. Homma, P. Finnie, Photoluminescence from single-walled carbon nanotubes: a comparison between suspended and micelle-encapsulated nanotubes, *Applied Physics A* 78 (2004) 1107 - 1110.
- [47] J. Lefebvre, J. M. Fraser, P. Finnie, Y. Homma, Photoluminescence from an individual single-walled carbon nanotube, *Phys. Rev. B* 69 (2004) 075403/1 - 075403/5.
- [48] V. C. Moore, M. S. Strano, E. H. Haroz, R. H. Hauge, R. E. Smalley, Individually suspended single-walled carbon nanotubes in various surfactants, *Nano Lett.* 3 (2003) 1379 - 1382.
- [49] M. Zheng, A. Jagota, E. D. Semke, B. A. Diner, R. S. McClean, S. R. Lustig, R. E. Richardson, N. G. Tassi, DNA-assisted dispersion and separation of carbon nanotubes, *Nature Mater.* 2 (2003) 338 - 342.
- [50] P. Cherukuri, S. M. Bachilo, S. H. Litovsky, R. B. Weisman, Near-infrared fluorescence microscopy of single-walled carbon nanotubes in phagocytic cells, *J. Am. Chem. Soc.* 126 (2004) 15638 - 15639.
- [51] A. Hartschuh, H. N. Pedrosa, L. Novotny, T. D. Krauss, Simultaneous fluorescence and Raman scattering from single carbon nanotubes, *Science* 301 (2003) 1354 - 1356.

- [52] D. A. Tsyboulski, S. M. Bachilo, R. B. Weisman, Versatile Visualization of Individual Single-Walled Carbon Nanotubes with Near-Infrared Fluorescence Microscopy, *Nano Lett.* 5 (2005) 975 - 979.
- [53] H. Htoon, M. J. O'Connell, P. J. Cox, S. K. Doorn, V. I. Klimov, Low Temperature Emission Spectra of Individual Single-Walled Carbon Nanotubes: Multiplicity of Subspecies within Single-Species Nanotube Ensembles, *Phys. Rev. Lett.* 93 (2004) 027401/1 - 027401/4.
- [54] J. Wu, W. Walukiewicz, W. Shan, E. Bourret-Courchesne, J. W. Ager III, K. M. Yu, E. E. Haller, K. Kissell, S. M. Bachilo, R. B. Weisman, R. E. Smalley, Structure-dependent hydrostatic deformation potentials of individual single-walled carbon nanotubes, *Phys. Rev. Lett.* 93 (2005) 017404/1 - 017404/4.
- [55] C. D. Spataru, S. Ismail-Beigi, L. X. Benedict, S. G. Louie, Quasiparticle energies, excitonic effects and optical absorption spectra of small-diameter single-walled carbon nanotubes, *Applied Physics A* 78 (2004) 1129 - 1136.
- [56] T. Ando, Excitons in carbon nanotubes revisited: dependence on diameter, Aharonov-Bohm flux, and strain, *J. Phys. Soc. Jpn.* 73 (2004) 3351 - 3363.
- [57] R. B. Weisman, S. M. Bachilo, Dependence of optical transition energies on structure for single-walled carbon nanotubes in aqueous suspension: an empirical Kataura plot, *Nano Lett.* 3 (2003) 1235 - 1238.
- [58] M. S. Dresselhaus, G. Dresselhaus, A. Jorio, A. G. Souza Filho, M. A. Pimenta, R. Saito, Single nanotube Raman spectroscopy, *Acc. Chem. Res.* 35 (2002) 1070 - 1078.
- [59] M. Zheng, A. Jagota, M. S. Strano, A. P. Santos, P. W. Barone, S. G. Chou, B. A. Diner, M. S. Dresselhaus, R. S. McIean, G. B. Onoa, G. G. Samsonidze, E. D. Semke, M. L. Usrey, D. J. Walls, Structure-based carbon nanotube sorting by sequence-dependent DNA assembly, *Science* 302 (2003) 1545 - 1548.

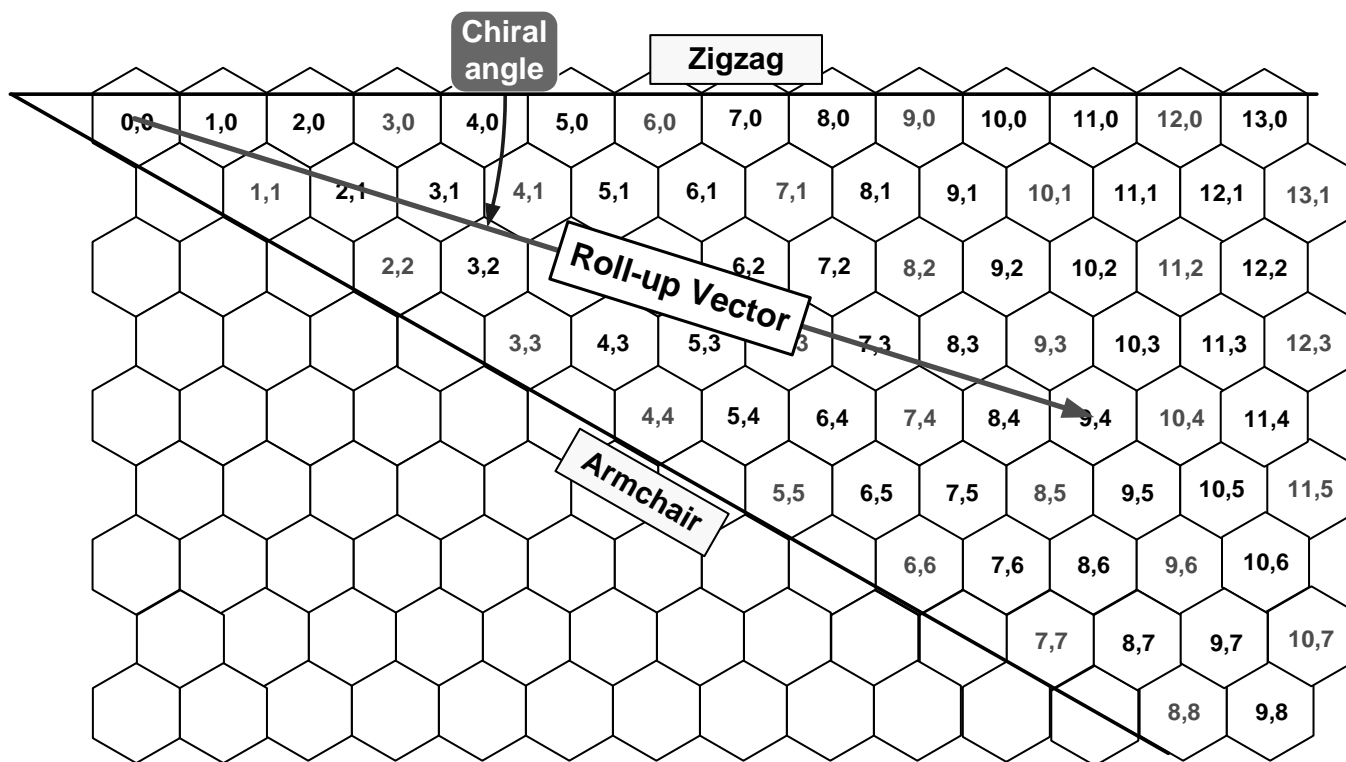


Fig. 1. Graphene sheet map illustrating possible single-walled nanotube structures that can be formed by wrapping the sheet to form a cylindrical tube. The resulting nanotube is labeled by the pair of integers in the cell that becomes overlapped with the origin cell. The nanotube's diameter is the length of the roll-up vector divided by π , and its chiral angle can lie between 0° (zigzag) and 30° (armchair).

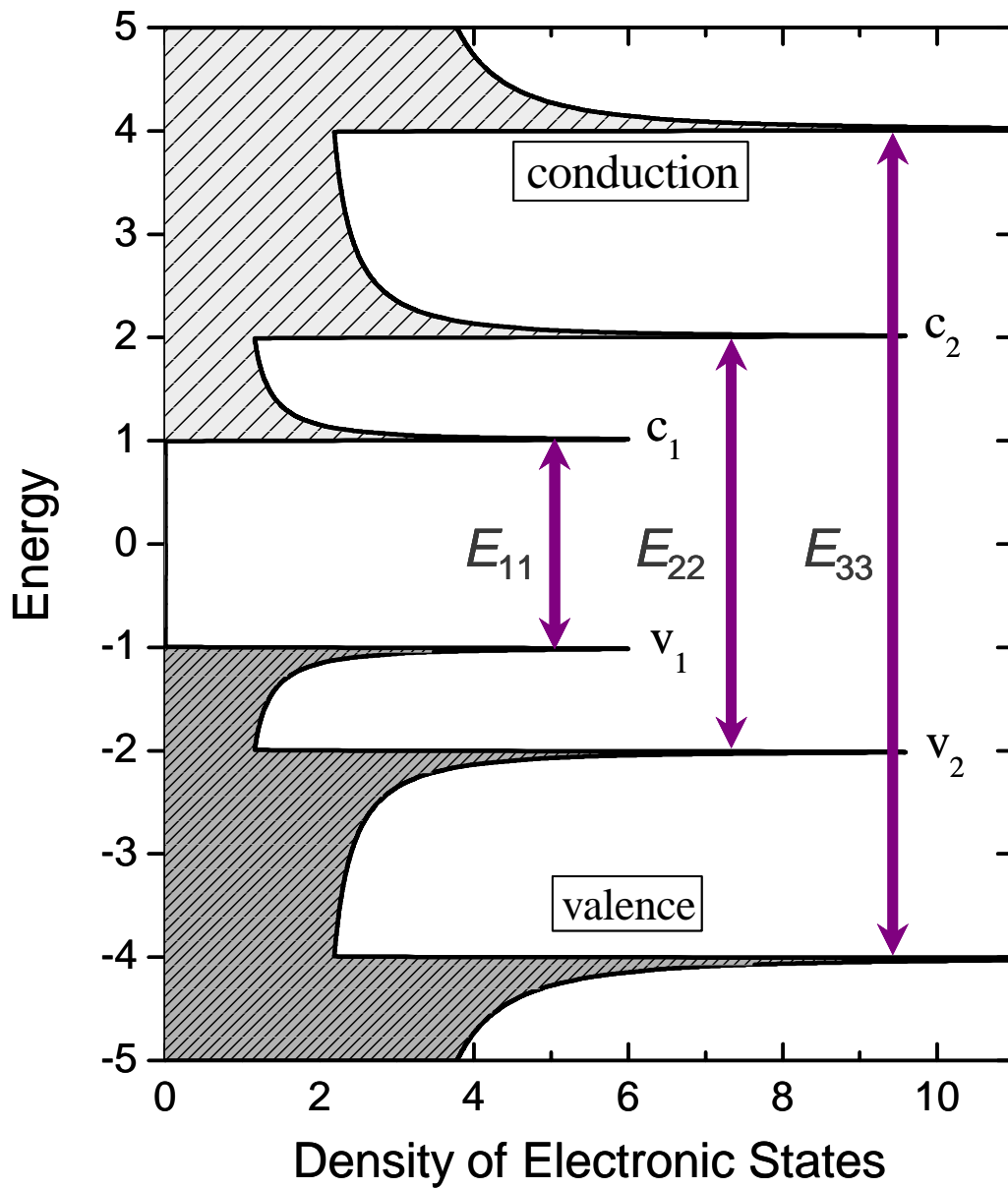


Fig. 2. Schematic density of states diagram for a semiconducting single-walled carbon nanotube, in a simple band theory model. Allowed optical transitions are illustrated as vertical arrows.

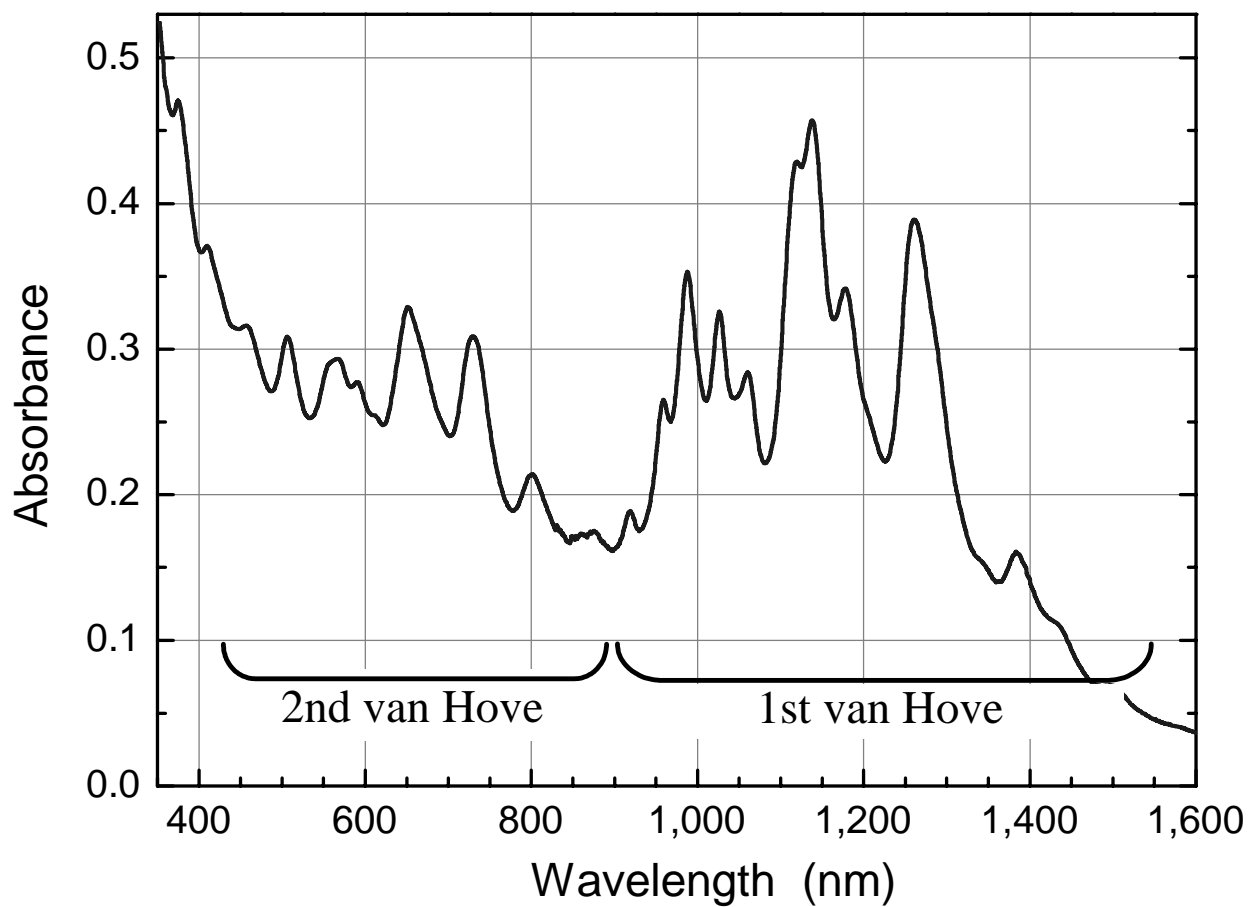


Fig. 3. Optical absorption spectrum of a sample of HiPco single-walled carbon nanotubes suspended in D₂O by SDS surfactant at 276 K.

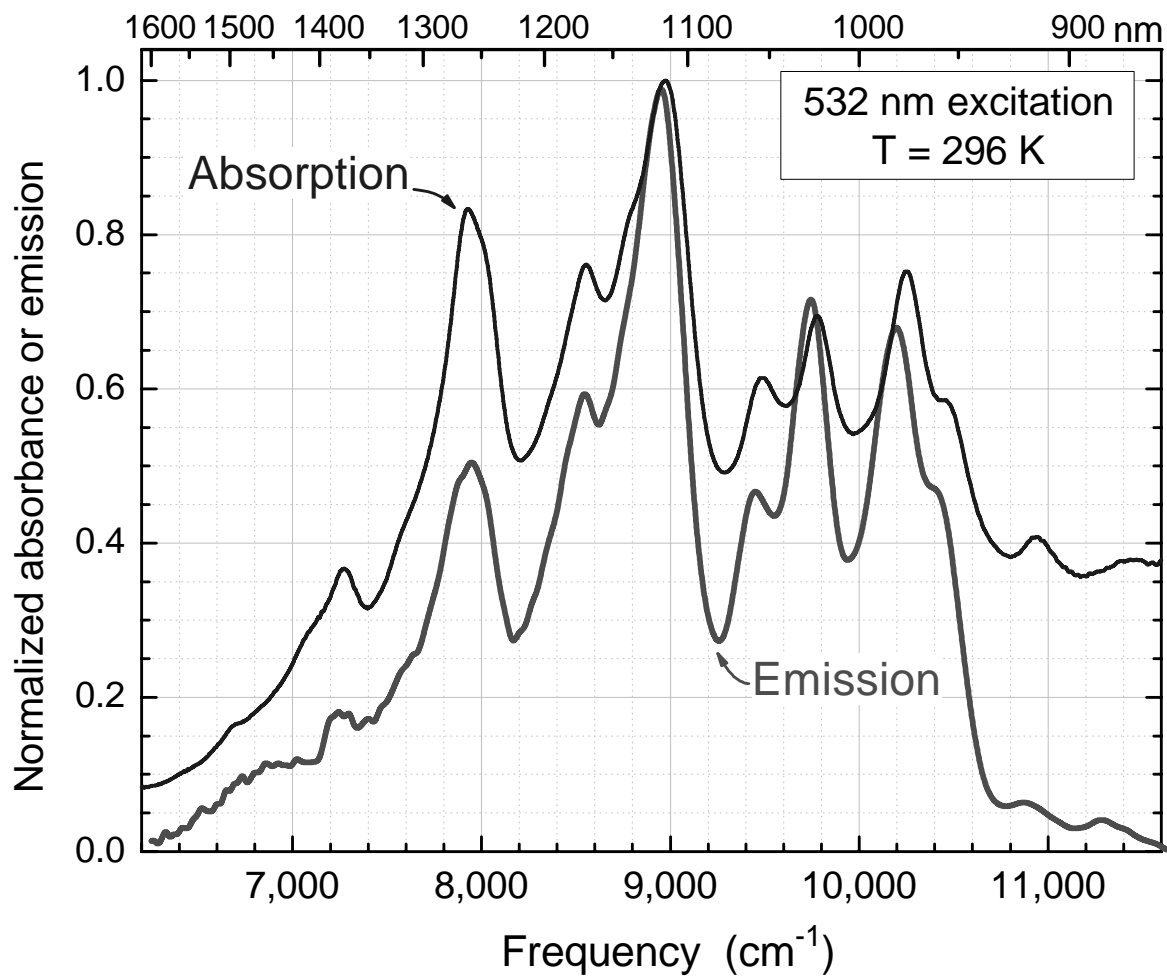


Fig. 4. Overlaid absorption and emission spectra of a sample of HiPco nanotubes in SDS / D₂O suspension. The emission was excited by a pulsed laser at 532 nm.

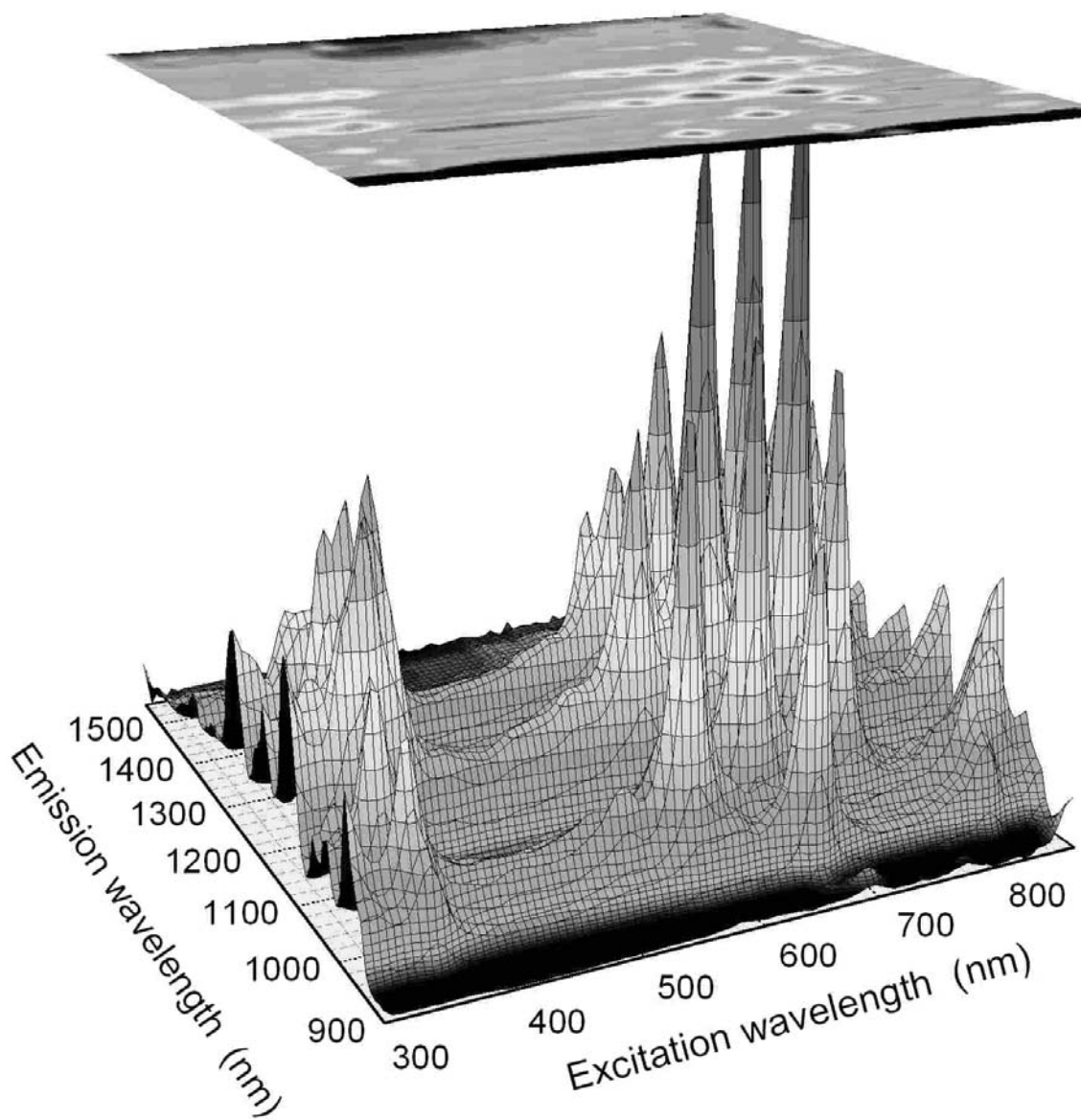


Fig. 5. Surface plot showing emission intensity from a sample of HiPco SWNT in SDS / D₂O suspension as a function of excitation and emission wavelengths. Each distinct peak arises from a specific (n,m) species of semiconducting nanotube.

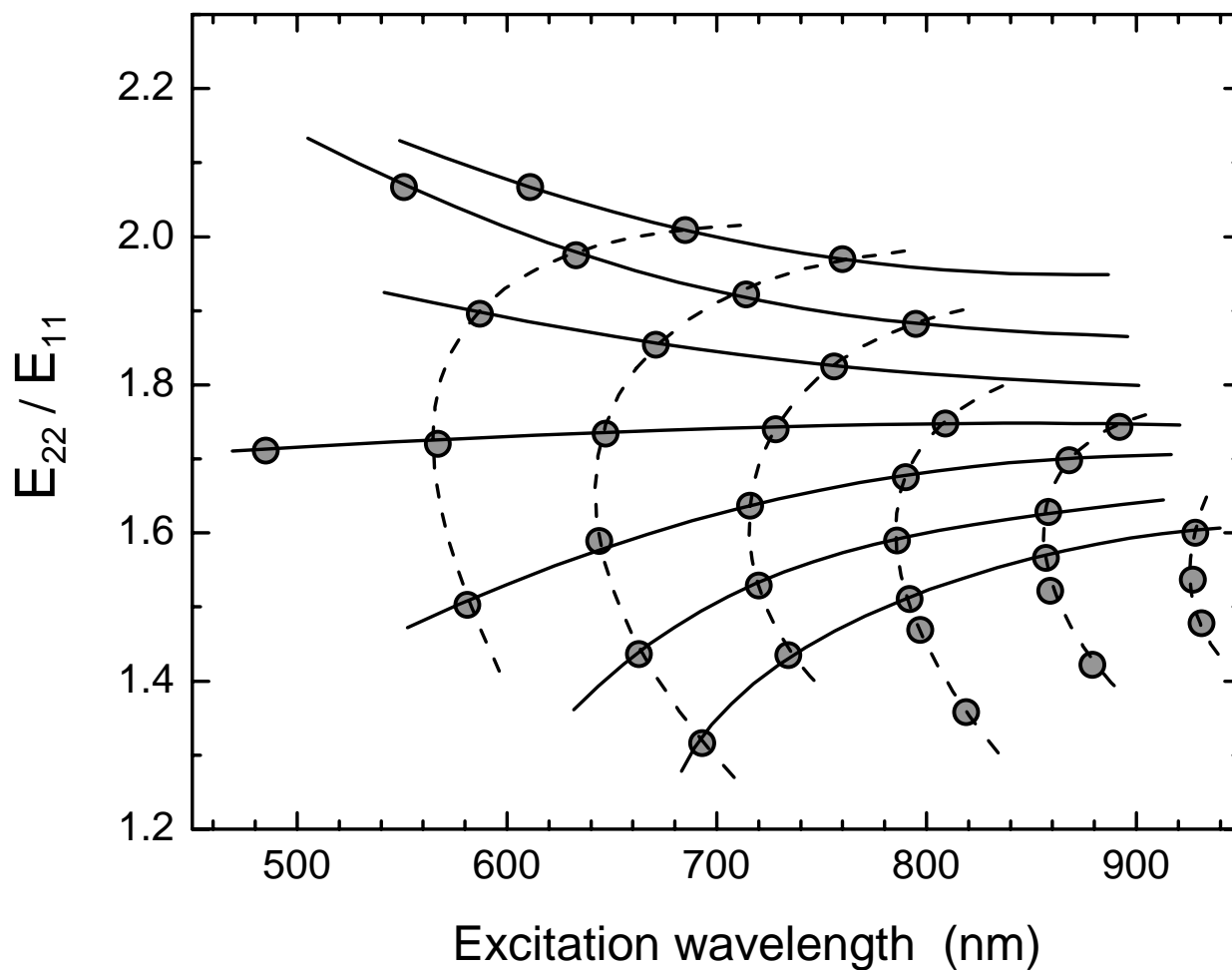


Fig. 6. Plot of the experimental photon energy ratios for excitation compared to emission as a function of excitation wavelength. The sample contained HiPco nanotubes in aqueous suspension. Points are measured values; lines indicate systematic patterns in the data.

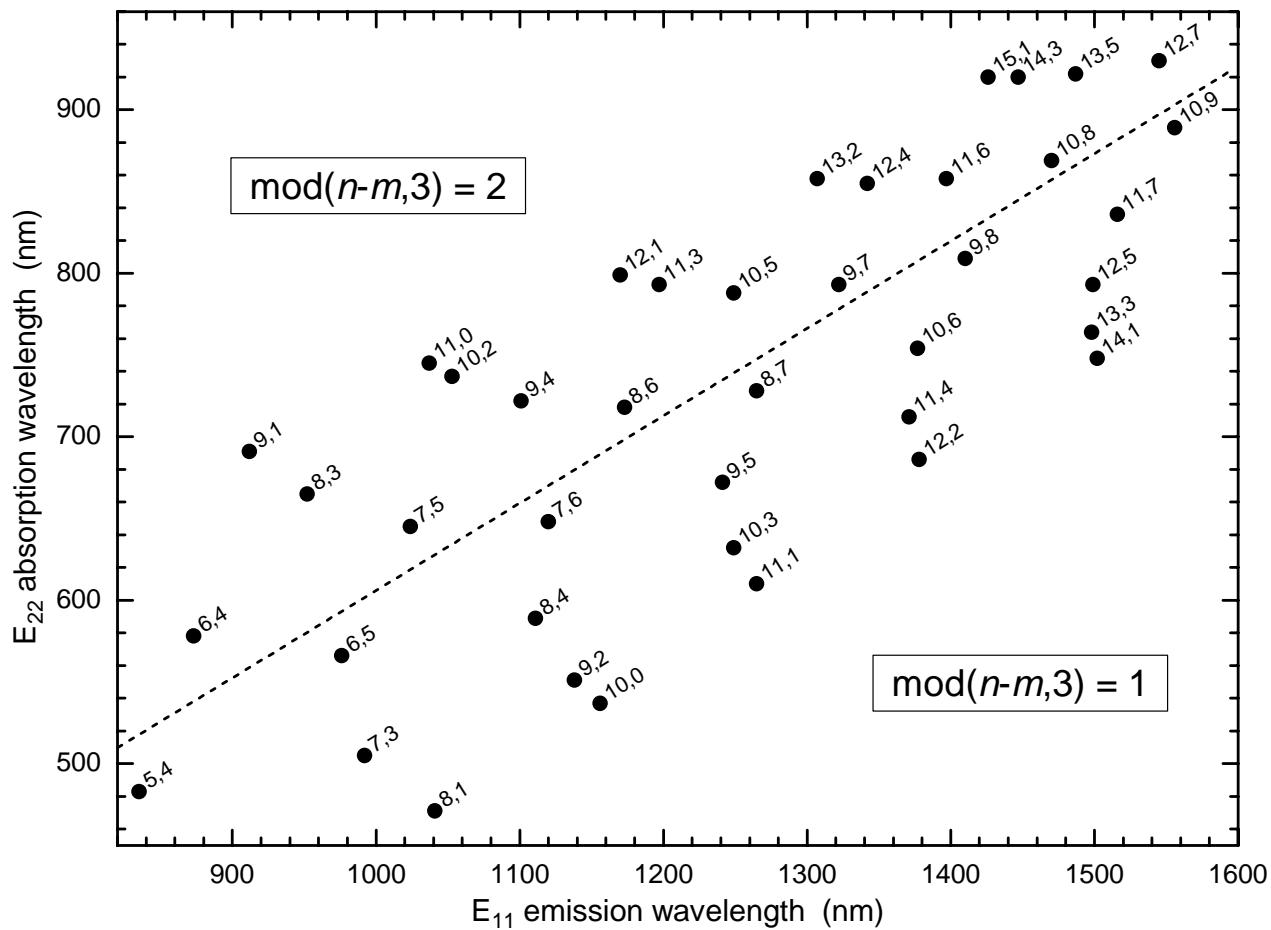


Fig. 7. Plot showing E₂₂ absorption wavelengths and E₁₁ emission wavelengths for a variety of SWNT in SDS aqueous suspension. Values are based on experimental measurements. The dashed line separates regions of “mod 2” and “mod 1” species.

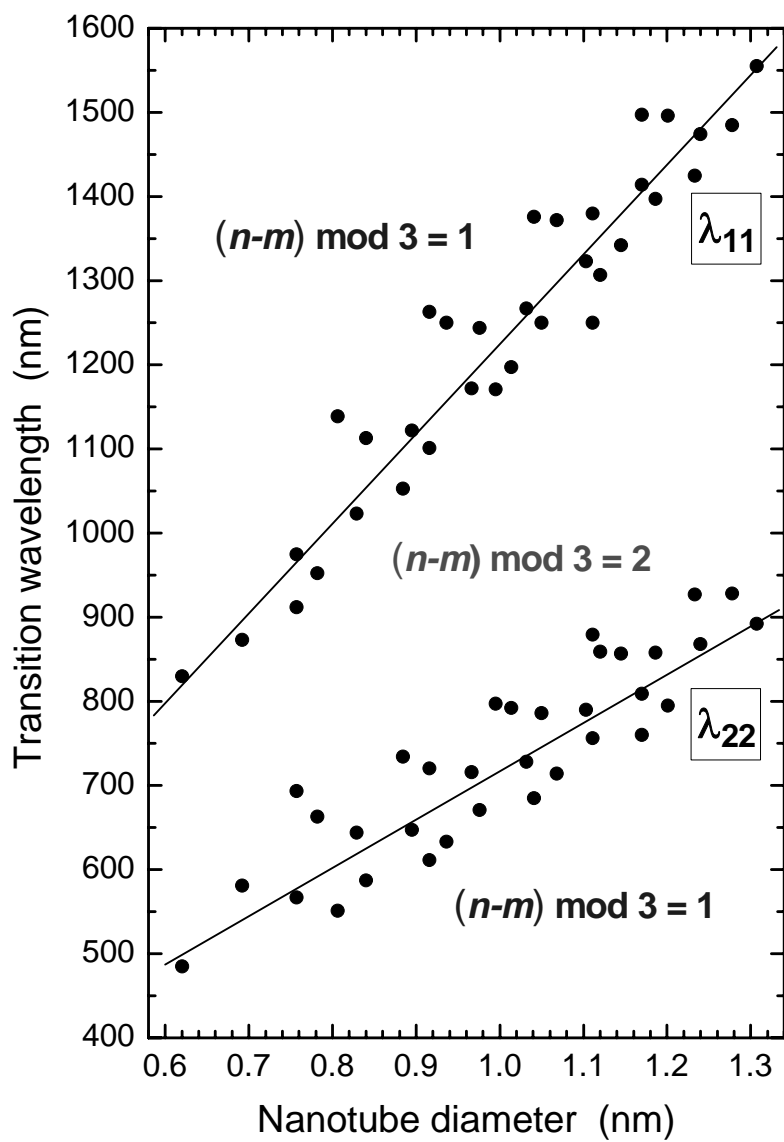


Fig. 8. Plot showing experimental wavelengths of E_{11} and E_{22} transitions in a sample of HiPco nanotubes in SDS / D_2O suspension. Solid lines separate regions of “mod 1” and “mod 2” species.

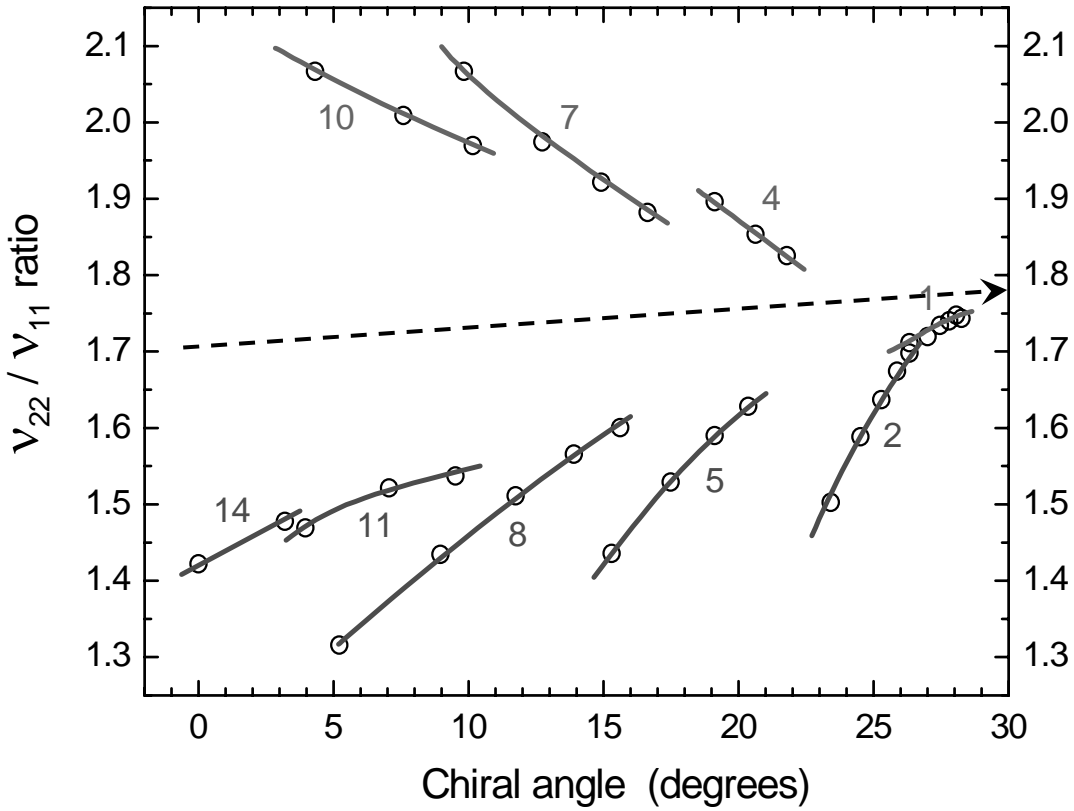


Fig. 9. Plot of the measured ratio of excitation to emission frequencies vs. nanotube chiral angle for SWNT in SDS / D₂O suspension. The points show experimental data and the lines connect points for species in the same $(n-m)$ family. Labels show those $(n-m)$ values. The dashed line illustrates an extrapolation of the ratio trend to the armchair limit of 30°. A limiting ratio of approximately 1.8 is indicated.

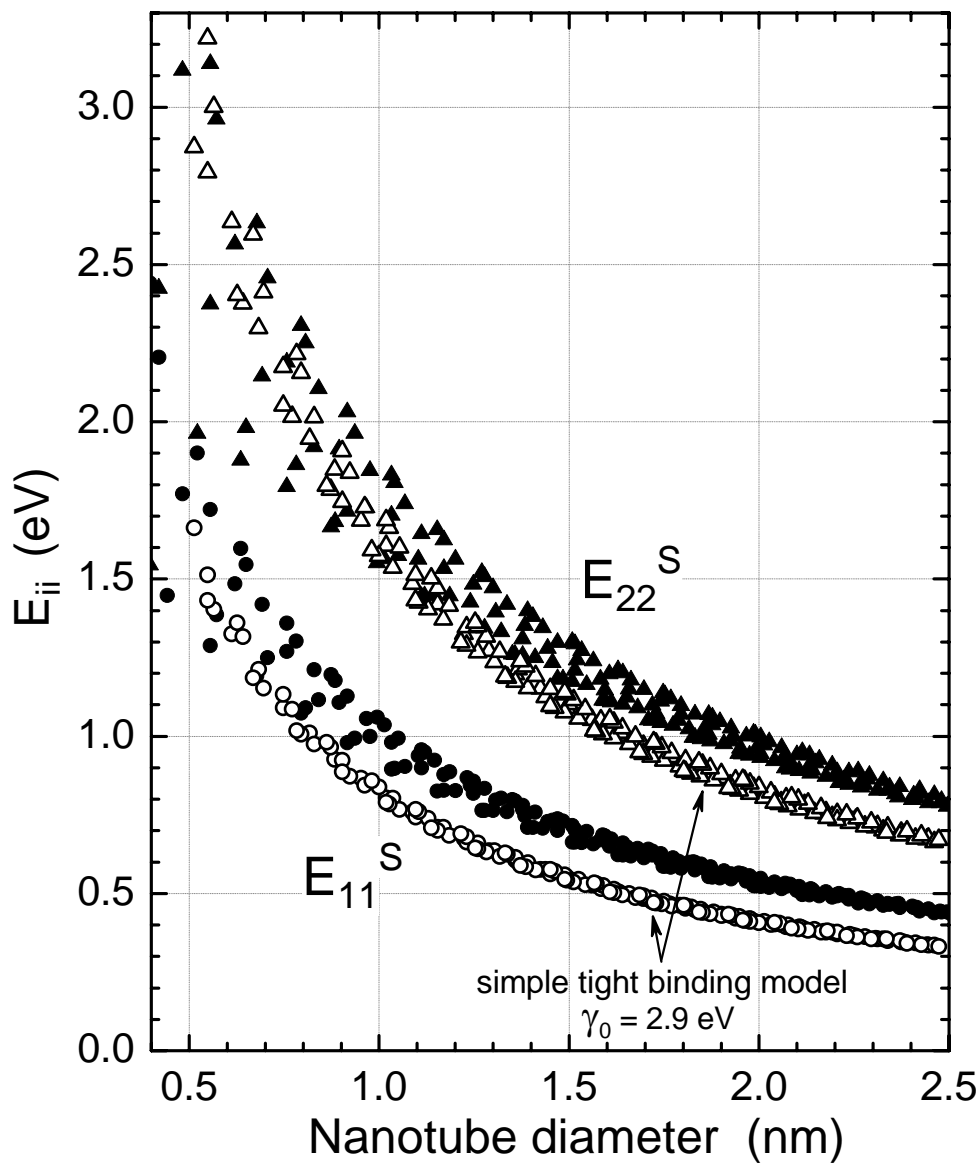


Fig. 10. Comparative “Kataura plots” showing optical transition energies as a function of nanotube diameter for the first and second van Hove transitions of semiconducting SNWT. Solid symbols are precise empirical extrapolations of experimental values, and open symbols are values computed using the simple tight binding model. Adjustment of the γ_0 parameter cannot bring the model into agreement with experiment.

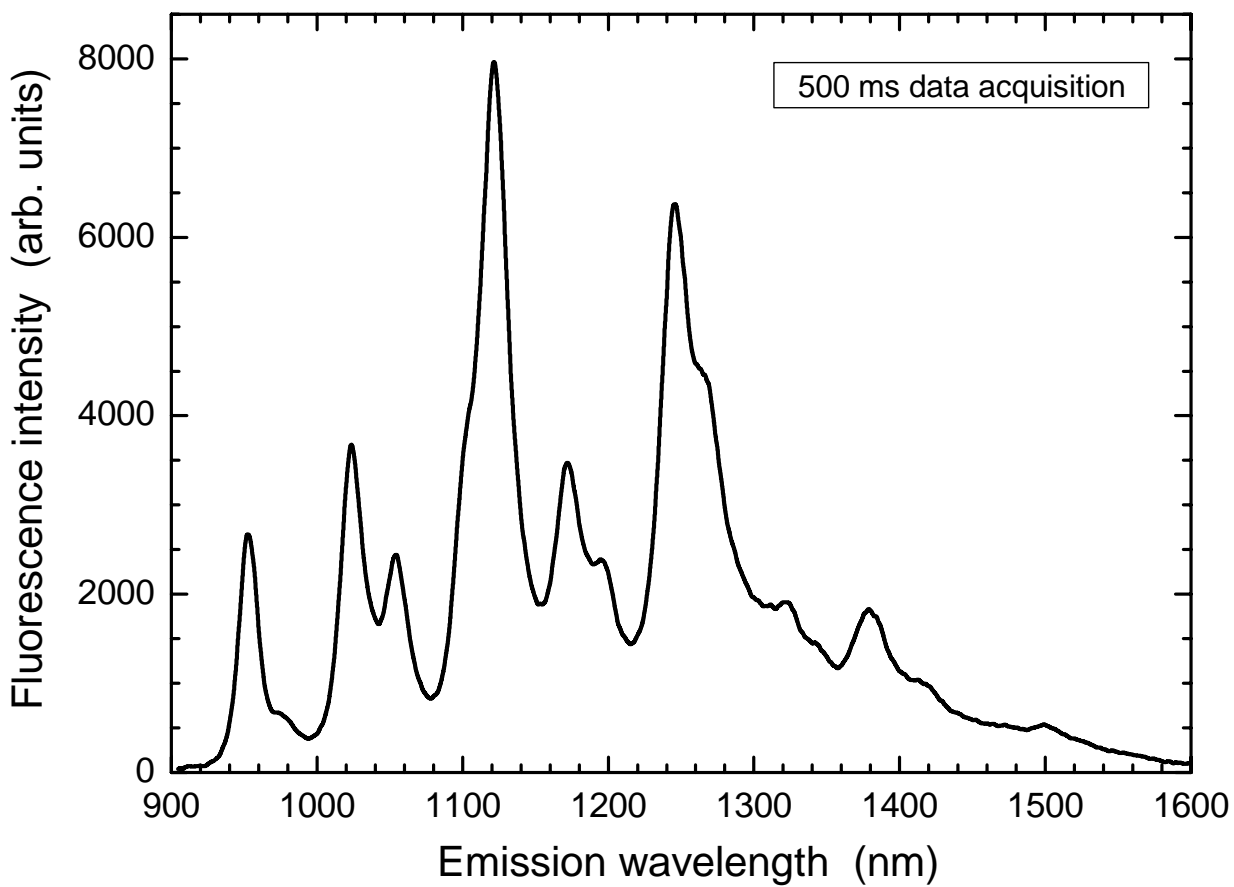


Fig. 11. Emission spectrum measured from a suspension of HiPco nanotubes in aqueous SDBS suspension using 658 nm excitation. The data were collected in 500 ms using an instrument designed for efficient fluorimetric analysis of nanotube samples. (Figure courtesy of Applied NanoFluorescence, LLC)

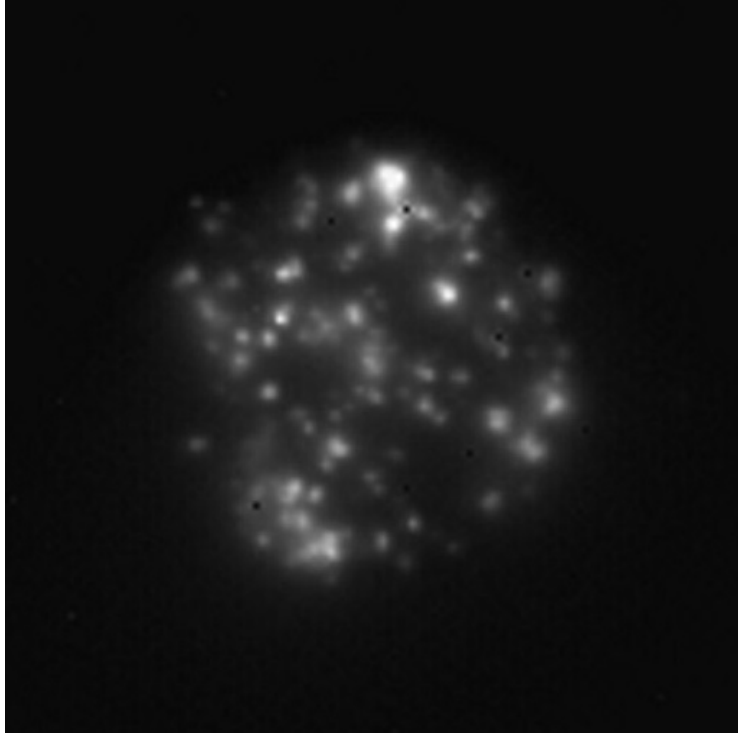


Fig. 12. Near-infrared fluorescence micrograph of a single macrophage-like cell that had been incubated in a growth medium containing suspended SWNT. The sample was excited at 658 nm and the image shows emission at wavelengths between 1125 and 1600 nm. The only significant emission under these conditions is from ingested nanotubes. The cell's diameter is approximately 25 μm .